Research Article

Szymon Oryński, Sebastian Kowalczyk*, and Bartosz Owoc

Ground penetrating radar and magnetic gradient distribution approach for subsurface investigation of solution pipes in post-glacial settings

https://doi.org/10.1515/geo-2022-0484
received January 05, 2023; accepted April 26, 2023

Abstract: Solution pipes are an important geomorphological feature in carbonate rocks formed by the host rock's dissolution due to water's focused flow, indicating the phenomena of water focusing in particular areas. However, their visual exposures are often limited by sediment and vegetation cover, making it challenging to understand their spatial distribution and morphology. In this study, we used geophysical methods such as ground penetrating radar (GPR) and magnetic gradiometer to detect and estimate the spatial distribution of solution pipes in a freshly exposed quarry site in Smerdyna, Poland. Our results indicate that both GPR and magnetometric measurements effectively detect most of the solution pipes, particularly those filled with large amounts of clay and silt particles. The GPR method, in particular, proved to be convenient due to the high contrast of the dielectric constant. The information on the positions and shapes of the pipes obtained based on these methods is crucial in understanding the link between pipe morphology and the physical conditions at the time of their formation. Furthermore, our measurements provided quasi-spatial correlations between pipe positions, the distribution of inter-pipe distances, and the potential relationship between alignments of rock joints and pipe locations. Our study demonstrates the potential of geophysical methods in detecting and understanding solution pipes, which are essential from environmental and climatic perspectives. This information can be used for future studies on pipe formation and environmental impact.

Keywords: ground penetrating radar, magnetic gradiometer, solution pipes, epikarst

1 Introduction

Epikarst, a skin of karst [1], is a weathered zone of enhanced porosity, usually near the soil/bedrock contact [2]. It is also a very fragile zone, which can be easily eroded or destroyed, on the one hand, and contaminated on the other. It is a zone associated with a number of natural risks, such as sinkhole development or ground subsidence, which is a hazard to anthropogenic structures.

Reliable characterisation of the epikarst system is critical for understanding its hydrological dynamics, groundwater vulnerability, and risk assessment of potential hazards. However, epikarst is difficult to characterise, despite its proximity to the surface. This is due to several factors. First, epikarst is highly heterogeneous, with many features at all scales, from large funnels down to small caverns, karst pockets, and solution pipes. Second, epikarstic components are usually covered with the soil or sediment layer, which limits direct observations to outcrops, except where the soil has been completely eroded. Hence, one is forced to resort to indirect methods of karst detection, in particular with the use of geophysical techniques [3–7], such as microgravimetry and magnetometry, DC-resistivity methods – mainly electrical resistivity tomography; and other electromagnetic methods, ground conductivity meter – slingram, very-low-frequency technique, time domain electromagnetic and ground penetrating radar (GPR), and a wide range of seismic methods (see ref. [5] for an overview of the most popular techniques). These methods have been typically used to detect features such as caves, larger conduits or collapse valleys [5,8,9]. However, smaller structures, such as pinnacles or notches, have also been detected [6,10,11]. Here, we apply GPR and vertical magnetic gradient (gradiometry) techniques to detect relatively

* **Corresponding author: Sebastian Kowalczyk,** Faculty of Geology, University of Warsaw, Warsaw, Poland,
e-mail: s.kowalczyk@uw.edu.pl
Szymon Oryński, Bartosz Owoc: Institute of Geophysics, Polish Academy of Sciences, Warsaw, Poland

small solution pipes (~0.5 m in diameter) that usually have numerous epikarst features and important water conduits to the subsurface. Solution pipes are karst geomorphological features formed in carbonate rocks with matrix porosity. The pipes appear as tubular vertical or near-vertical cavities in the epikarst zone. They vary in size and can be over 100 m deep and over 10 m in diameter, but the most common are depths between 1 and 4 m and diameters between 20 and 80 cm [12]. Challenges in characterisation and mapping of solution pipes were mentioned by Lipar et al. [13].

Information about the internal structure of shallow deposits can be obtained with the GPR measurements, providing non-invasive high-resolution and continuous electromagnetic wavefield images (radargrams). The GPR method has been successfully applied to investigate the internal architecture of limestone [14,15], limestone gallery network [16], or karst features [14,17–24]. The ability of GPR to map cylindrical vertical karst structures, including solution pipes, was tested several times [17–23]. These studies have not always produced precise results, and not all objects are detected. Sometimes, larger pipes are only suggested [19,23]. Successful recognition of solution pipes by GPR probably depends on several factors, such as the size of the solution pipes, the antenna frequency, the overburden thickness, and the contrast of electrical properties between the material filling the solution pipes and the rock.

Additional information about shallow deposits can also be obtained by gradiometers, the instruments designed to measure gradients of Earth's magnetic field. It is possible to determine horizontal gradients [25]. However, only the vertical component was used in this research as it is easier to process. In the ground version of gradiometers, the distance between sensors should be between 0.5 and 1.5 m [26]. As the vertical gradient is measured, noise effects from long-wavelength magnetic fields are suppressed, and only anomalies from external sources are amplified. All magnetic datasets contain elements of disturbances and artificial noise; therefore, they require diurnal correction. The most significant correction is the diurnal variation in the Earth's magnetic field. However, the obtained data can be adjusted by measuring only the gradient and not the absolute value of the magnetic field. The gradient is determined by subtracting the measurement results between the two sensors. Thus, the diurnal variation is automatically corrected as it has the same effect on both measurements [27]. The gradient of the dipole magnetic field is inversely proportional to the fourth power of the object's distance from the measuring station to the source of this field [28]. Thus, as the depth of the anomaly source increases, the value of the measured gradient decreases rapidly. When measuring the magnetic field using the gradient method, direct information about shallow objects, at the level from a few to several metres below the ground surface, is obtained [29]. The influence of the regional field associated with more profound and extensive anomalies is negligible.

This study tested the geophysical approach of detecting solution pipes using GPR and gradiometers. We analyse the detection capability of these methods in terms of pipe locations, distribution, and morphology by comparing the predictions with the field data. We chose a freshly exposed quarry site, which allowed us to test this approach in a latitudinal cross-section with visible pipes to verify the results. An example of a solution pipe from the investigated quarry is shown in Figure 1.

2 Geological setting

The research area is located in the surroundings of Smerdyna village, roughly 12 km east of Staszów in southeastern Poland (Figure 2a), in a temperate warm transitional climatic zone with increased continental impact [30]. Mining activities provided extensive exposure to Middle Miocene calcarenite with

Figure 1: An example of a solution pipe on the walls of the Smerdyna quarry.

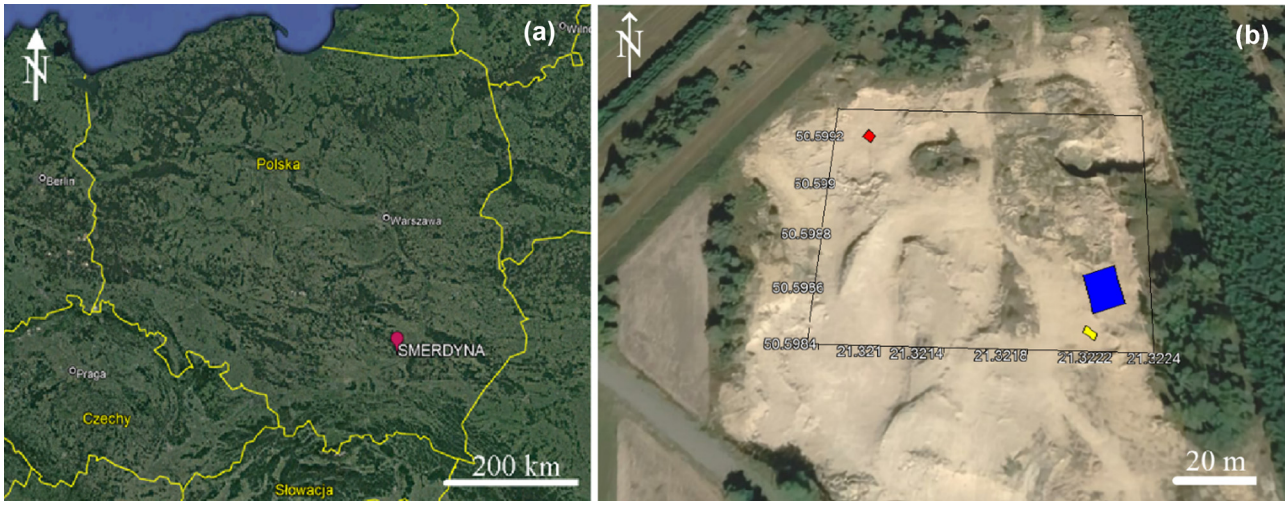

Figure 2: The locality of the research area. Location of the study area on the map of Poland (a). The satellite image of the grids inside the quarry (red – Grid 1; yellow – Grid 2; blue – Grid 3) (b).

the presence of solution pipes. The calcarenite is part of the Chmielnik formation [31], representing a range of quartz-rich sandstones and calcarenites of post-collisional deposition on the basin forebulge flank [32]. The bioclastic white to pale grey calcarenites around Smerdyna exceed 90% carbonate content and mainly contain quartz residues, followed by illite and smectite clay minerals [33]. The calcarenites are fractured and cross-bedded; their cross-beds are angled up to 27° with only a few degrees of post-depositional tilting [33,34]. The total porosity is estimated to be 36% [35]. The calcarenites are overlain by up to 5 m of uncemented Pleistocene glacial tills [36] from which the material for filling solution pipe is derived [33].

The solution pipes were described first in the quarry where the surveys were conducted [37,38] as karst forms filled with brown weathered material. Mycielska [37] indicated that these fillings are made of glacial tills. Later, research from Mycielska-Dowgiałło [38] allowed for the extension of this information and it was concluded that the karst structures are also filled with various sediments. White and dusty lime sediment is at the bottom of the solution pipes, and above is a reddish-brown weathered material (Terra Rossa). Sometimes, sand inserts are visible between the streaks of the weathered layer. Then, there are Pleistocene formations made of sand with clay at the bottom above the clay. According to Mycielska-Dowgiałło [38], the boundary between red-brown (Terra Rossa) and sand-brown weathered materials is often blurred. Many solution pipes were found in the investigated quarries in longitudinal and lateral cross-sections. Morawiecka and Walsh [39] and Walsh and Morawiecka-Zacharz [33] published a detailed study of solution pipes in this locality, including lithological characteristics of this area. The average depth of the pipes is 1.9 m, and the average diameter is 0.6 m. Their formation is most likely related to releasing a large amount of water during the Elsterian deglaciation (~450–400k year ago) [12,33]. Based on the surrounding walls of the quarry, around 2 m of limestone was removed from the analysed surface.

3 Materials and methods

GPR and gradiometry measurements were carried out on three different polygonal grids on the freshly excavated ground of the quarry (Figure 2b). The bottom of the quarry was heavily altered and the ground was disturbed as a result of calcarenite extraction. Here and there, areas where solution pipes could potentially be located were visible – darker or brighter material appeared, scattered irregularly nearby. The area (Grids 1 and 2) was selected in such a way that the searched structures were visible, i.e. there were indications of the occurrence of solution pipes. At Grid 3, the quarry floor was covered with a heavily altered layer of sand and clay, and the ground was disturbed as a result of calcarenite extraction. The location of the solution pipes was confirmed after geophysical measurements, when the covering layer was removed with a shovel (Grids 1 and 2) or an excavator (Grid 3).

Grid 1, with dimensions of 2.8 m × 3.5 m, was focused on a single large solution pipe. Grid 2, 1.8 m × 3.5 m in size, was aimed at two solution pipes with different

fillings. In addition, one of the pipes was situated at the edge of the grid in such a way that only half of its horizontal circular area was measured. At Grid 1 and Grid 2, solution pipes were visible, i.e. there were indications of the occurrence of solution pipes on the quarry floor prior to the GPR and gradiometry survey. This allowed us to check how the instruments detected their presence. Grid 3 was the largest, 11.5 m × 12.5 m in size, and contained visually identified pipes of various sizes and fillings. The methodological assumption of the conducted geophysical measurements was to test their effectiveness in places where the presence of solution pipes (Grids 1 and 2) was suspected and then to apply these methods in the areas where there were no indications that solution pipes were present below (Grid 3). In terms of methodology, Grid 2 was particularly interesting, where indications of the occurrence of solution pipes were visible as dark and bright zones. Both geophysical surveys were performed on dense measurement grids. Measurement profiles were determined parallel to each other. On the largest grid (Grid 3), measurements were also made on perpendicular profiles. The GPR measurements were acquired for the assumed length of each profile. In comparison, the magnetic gradiometry measurements on each profile were made with a time-step approach along more or less the same lines as the GPR with the determination of the exact position according to its internal global positioning system (GPS).

3.1 GPR

The GPR measurements acquired a total of 15 lines for Grid 1, 10 lines for Grid 2, and 57 X and 69 Y lines for Grid 3. GPR profiles were determined parallel to each other at a distance of 0.2 m. The real distance between the Y profile lines on Grid 3 turned out to be smaller – the average distance is 0.18 m. The Malå Ground Explorer (GX) High Dynamic Range system with a shielded 450 MHz antenna was used during the surveys. The GPR data were collected using a trace distance interval of around 0.04 m and a sampling interval of 0.195 ns. The obtained GPR data were processed in ReflexW software [40] using multiple procedures to improve the signal-to-noise (S/N) ratio and correlate valuable reflections. The data were processed using the following steps: subtraction of the mean (dewow), moving the start time, gain function, bandpass filtering, background removal, and time cut. The data collected in the form of a 2D profile grid on the surface were used to create a 3D volume in Voxler software.

3.2 Magnetic gradiometer

Gradiometric measurements were conducted using the GEM GSM-19T Overhauser Magnetometer integrated with GPS. This allowed for measuring the total magnetic field with its location and vertical gradient. The latter was used in our analysis. The distance between the sensors for vertical gradient measurements was set to 0.96 m, within the recommended range for the ground version of gradiometers [26]. When a vertical gradient is measured, the noise effects from long-wavelength magnetic fields are suppressed. In particular, correcting the diurnal variations in the Earth's magnetic field is optional, as is the case for the total magnetic field data [27]. The gradient of the dipole magnetic field is inversely proportional to the fourth power of the object's distance from the measuring station to the source of this field. Therefore, as the depth of the anomaly source increases, the value of the measured gradient decreases rapidly. The measurement grids were similar to the GPR ones. The measurement was made every second along the profiles spaced 0.2 m apart. The marching time was adjusted in such a way that the measurement step along the profile was about 0.1 m. After filtering and processing, the data collected in the form of a 2D mesh on the surface were used to create a 2D vertical magnetic gradient distribution in Surfer software.

4 Results and discussion

4.1 Results by methods

4.1.1 GPR

The GPR radargrams show several strong reflectors and zones where the signal is attenuated. The reflectors are interpreted as the dipping boundaries of the calcarenite layers, while the zones of attenuated GPR reflectors are interpreted as solution pipes (more precisely, they correspond to the material filling the pipes). As is commonly known, the GPR signal's attenuation increases with the analysed material's electrical conductivity. In particular, highly conductive clays strongly weaken the electromagnetic waves emitted by the GPR. In contrast, the attenuation by calcarenites is significantly lower due to their smaller conductivity. Interestingly, Collins et al. [17] did not find a significant effect of sediment filling of the solution pipes on the GPR signal. However, in the areas of their research, they noted that there were no soils with

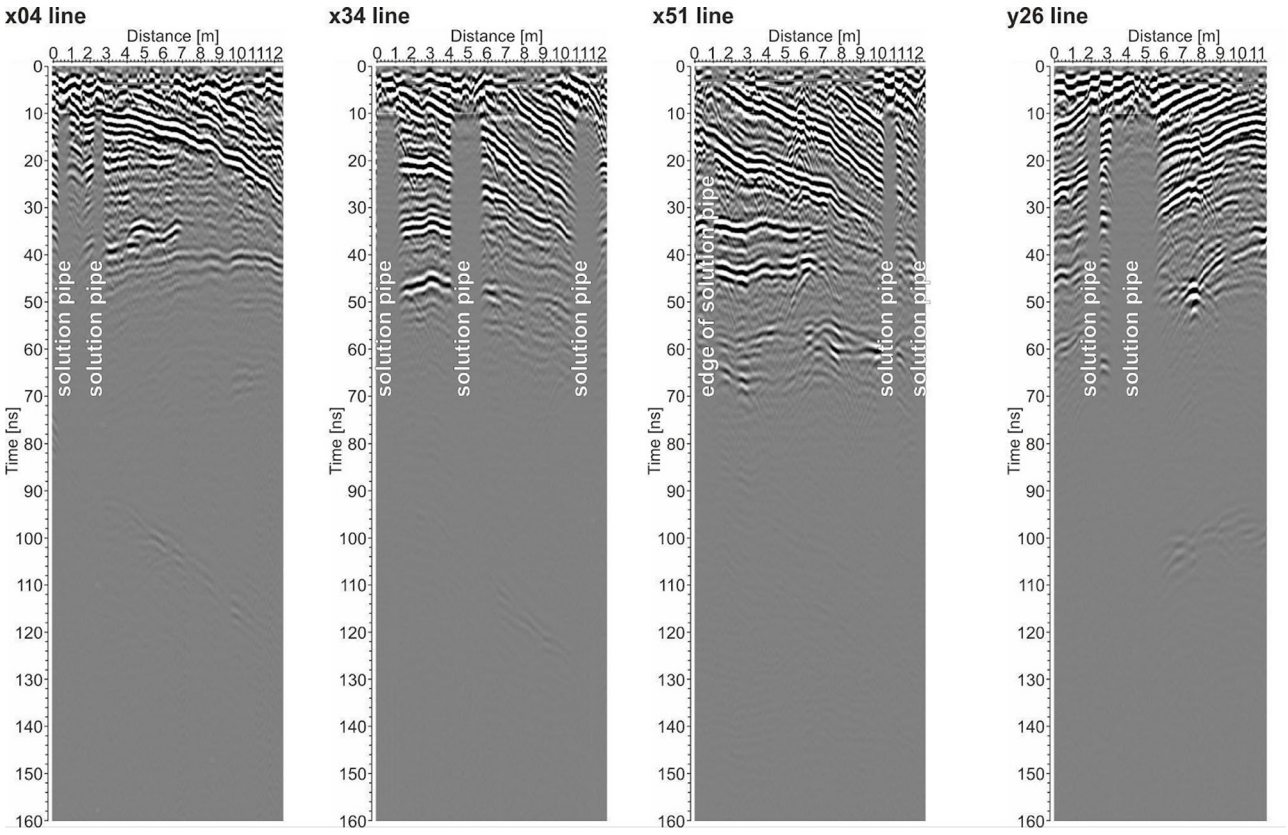

Figure 3: Radargrams with interpretation along the selected measuring lines (Grid 3).

properties commonly associated with limiting radar energy and probing depth. Comparing the research presented in this article and that of Collins et al. [17], several significant differences were noted. First, the measurements were conducted by completely different GPR instruments (technologically advanced reflects into better resolution) with a different antenna frequency, which is reflected in the resolution and the potential depth range ([17] – 120 MHz, these measurements – 450 MHz). Finally, and most importantly, our research areas differed significantly, especially in terms of the properties of the filling material of the solution pipes. In the Collins et al. [17] work, the percentage content of the particle size of silt and clay ranged from 7 to 35%. In Smerdyna, the filling material of the solution pipes was analysed macroscopically; however, samples filling two solution pipes on Grid 3 were tested in the laboratory. The results of hydrometer analysis indicate that this material consists of 40% clay fraction and 91% sum of clay and silt fraction. As noted by Collins et al. [17], the amount or proportion of clay necessary to have a negative influence on the radar performance is not known and that soil properties commonly associated with restricting radar energy and probing depth were not present in their two study plots. In the research areas presented in this article, clays filling solution pipes attenuated the energy of the radar signal. Therefore, we could not determine the depth range of solution pipes on the basis of radar energy. We used a methodology consisting of locating (only as x, y coordinates) structures with high electrical conductivity (solution pipes filled

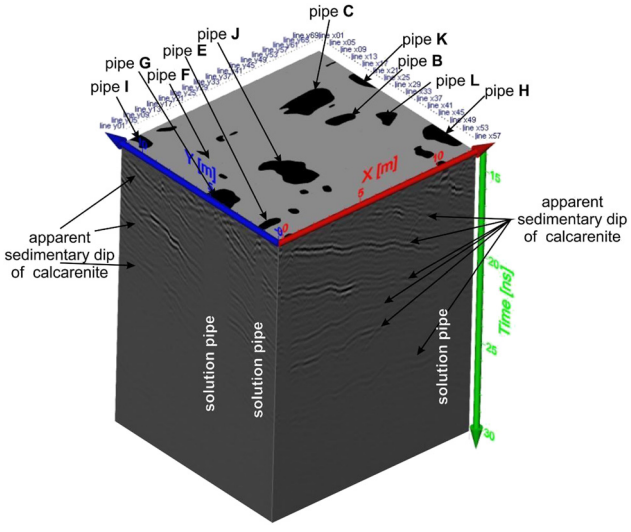

Figure 4: Spatial distribution of the reflected and attenuated GPR signals in the studied area (Grid 3).

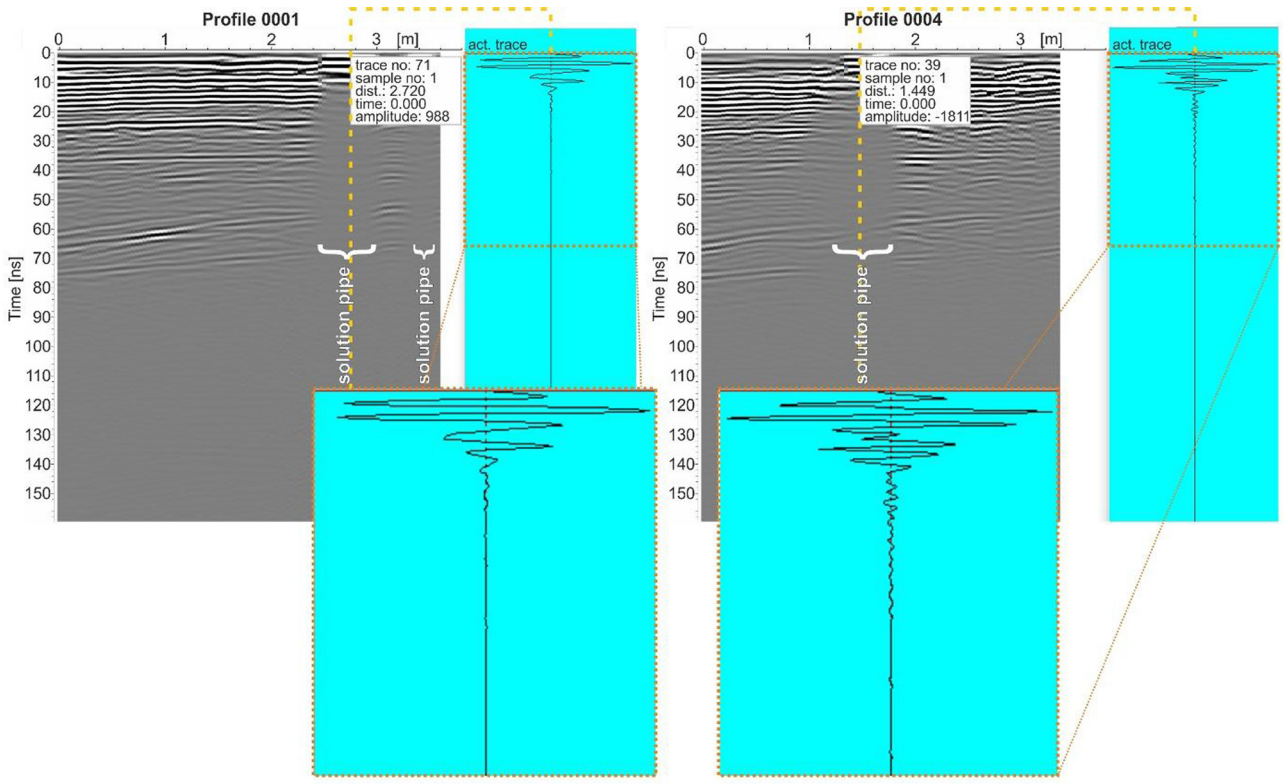

Figure 5: Radargrams obtained in Grid 2. The traces show different attenuation depending on the materials filling the solution pipes. The solution pipe beneath the GPR Profile 0001 is filled with more clayey and silty material, while that one below the GPR Profile 0004 is filled with more sandy material.

with clay) surrounded by rocks of low electrical conductivity (calcarenite). Such an approach (localization based on GPR signal attenuation and determining the depth range based on the electrical resistivity method) is applied, for example, in the study of contaminated areas or the technical condition of flood embankments.

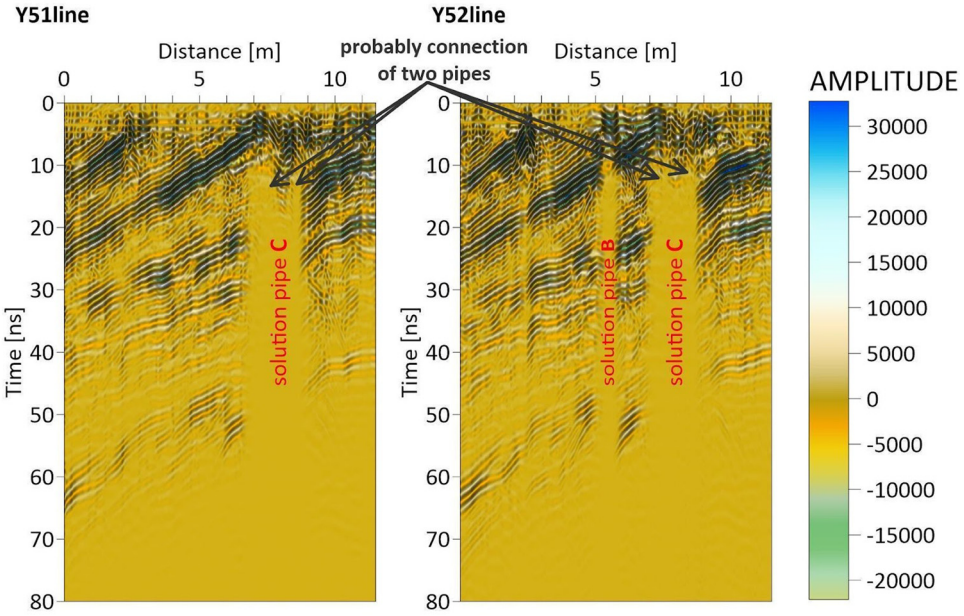

Figure 6: Radargrams showing reflected and attenuated signals with pipe positions (Grid 3).

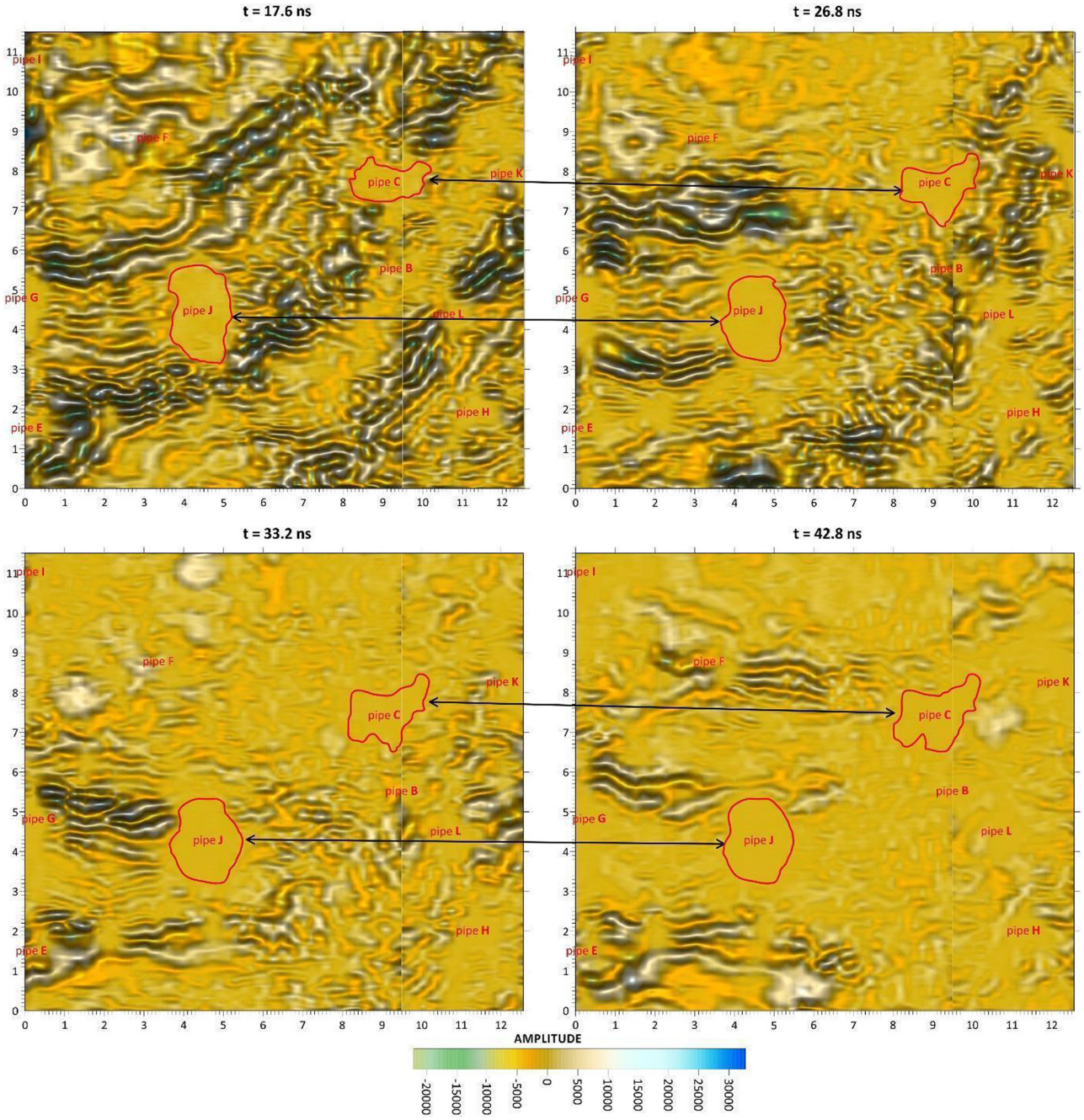

Figure 7: Time slices showing reflected and attenuated signals at different times with pipe positions in Grid 3. The values on the *x*, *y* axes are in metres.

Using this knowledge, their positions were marked on the 2D cross-section (Figure 3) and 3D model (Figure 4), indicating the location of the solution pipes in the investigated area. The presence of clay minerals does not completely weaken the radar signal, as they may not be the basic filling material of the examined structures. Several radargrams are presented in Figure 3. The zones of attenuated reflections associated with solution pipe fillings are clearly detectable. However, the attenuated signal does fade out entirely with depth, so the bottom of the pipes cannot be determined.

As mentioned before, the pipe filling material was subjected to *in situ* macroscopic analysis. The type of soil filling the solution pipe affects the propagation of the electromagnetic signal, and this can be easily seen in the single traces. To demonstrate this phenomenon,

the exemplary traces of the radargrams corresponding to different attenuation depending on the material filling the solution pipes are presented in Figure 5. The solution pipe beneath the GPR Profile 0001 (left side of the grid) is filled with more clayey and silty material. It shows a shorter penetration length of the electromagnetic signal than the GPR Profile 0004 (central part of the grid) with a pipe filled with more sandy material.

The shape of solution pipes is difficult to determine unequivocally based on GPR measurements. The GPR signal profiles do change with depth. An additional complication in interpreting their form may be the merging or apparent joining of two smaller pipes next to each other (Figure 6). Moreover, from what can be seen in the photos of the quarry walls (Figure 1), the pipes narrow with depth. However, this is not visible in the GPR images, mainly because the clays attenuate the propagation of electromagnetic waves. This leads to a complete decay of the GPR signal along with depth, so the deeper parts of the pipes, especially their bottom, may not be recognised. For deeper pipes, the changes in the shape of the pipes and the attenuation of the signal can be illustrated by time slices (Figure 7). The reduction of the pipe cross-section with depth, as shown in Figure 1, is not observed in the GPR images (Figures 3–7). This is most likely due to the signal attenuation by clay filling the pipes. Since solid attenuation of the electromagnetic signal by clay attenuates the electromagnetic wave propagation, the deeper parts of the pipes, especially the bottom parts, may fall beyond the detection range and not be detected. At larger times, we observe (Figure 7) broader horizontal cross-sections of the pipe at a given (x, y) coordinate. Thus, the reconstruction of the shape of the pipes is the most reliable in the early measuring times of their appearance in the GPR images. The detection of pipes for Grid 3, presented later in this article, was performed for a time of approx. 15 ns, i.e. just below the rubble layer constituting the quarry floor and covering the pipes.

Interestingly, the radargrams (Figure 6) show that above the part of the solution pipe marked as C (Grid 3), there are continuous reflections interpreted as the dipping of the calcarenite layer. Such an image of the occurrence of reflections above the attenuated signal was recorded for several measurement lines (Y50-Y53) on Grid 3. These radargrams suggest that for these several measurement lines, solution pipe C is narrower at the surface and later it widens. Since no detailed geological research has been conducted, it is difficult to clearly explain it. It is possible that this is the result of a very local change in the properties of the rock.

4.1.2 Magnetic gradiometer

The gradiometer consists of two magnetometers mounted vertically, placed in series, one above the other. The top

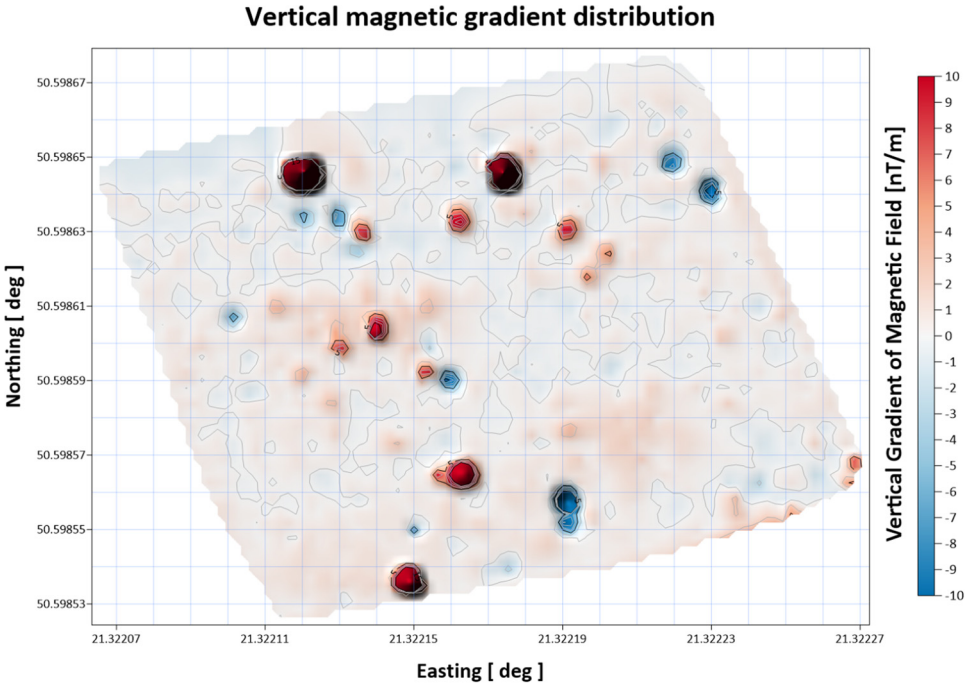

Figure 8: Spatial distribution of vertical magnetic gradient plotted in Smerdyna (Grid 3).

sensor measures predominantly the Earth's magnetic field, while the lower sensor is more affected by any localised magnetic anomalies connected with the presence of magnetic minerals. The difference between the sensors will relate to the strength of a magnetic field created by these minerals. The output of the device is the difference in magnetic flux at that point in space. In other words, the result is the difference between what each of the magnetometer measures. The magnetic effect diminishes with the third power of the distance, so positive gradient anomalies appear at the site of the occurrence of magnetic minerals. Magnetometric measurements at the quarry floor showed several positive (up to 10 nT/m) and negative (up to −10 nT/m) vertical gradients of the magnetic field. Positive anomalies should be caused by higher magnetic susceptibility related to a more significant amount of magnetic elements (in particular, iron and/or nickel) in the solution pipe fillings compared to the host rock. Figure 8 shows the result of magnetic gradiometry measurements in the largest studied area (Grid 3).

Additionally, we have compared our results to previous studies [38] in similar geological settings and found that the lack of a magnetic anomaly is not uncommon in clay-rich sediments. This could be due to a variety of factors, including the absence of magnetic minerals, the presence of non-magnetic clay minerals that mask any magnetic signal, or the effects of burial diagenesis on the magnetic properties of the sediment. The magnetic properties of clay depend on the presence of minerals that contain magnetic elements, such as iron, nickel, and cobalt [41]. The low values of the anomalies of the vertical magnetic gradient in the research area indicate small contents of magnetic minerals in the tested medium.

4.2 Results by areas

4.2.1 Grid 1

Grid 1 contains a single solution pipe filled with ferruginous silty loam, which was detected by both geophysical methods. There, the maximum of the positive magnetic anomaly coincides with the location of increased attenuation of the electromagnetic wave visible in the GPR image (Figure 9). This demonstrates that the attenuated reflections of the GPR signal and points with relatively high values of the magnetic gradient are correlated and indicate the presence of a sediment-filled solution pipe in the research area.

4.2.2 Grid 2

Grid 2 demonstrates that not all anomalies identified by GPR measurements as solution pipes are also detected by gradiometric surveying. This grid contains three solution pipes, as presented in Figure 10. The largest one (pipe B) is positioned in the centre of the grid and is filled with a sandy material that we identify as a core according to the classification of Walsh and Morawiecka-Zacharz [33]. This pipe was clearly visible in the GPR image but not in the magnetic data. The second (pipe A), a smaller solution pipe, was located in the northeastern part, at the edge of the grid and is visible both as a GPR anomaly and as a weak negative magnetic gradient anomaly. The filling material of this pipe was of dark colour and very compact. According to Walsh and Morawiecka-Zacharz [33], it is an example of a reddish-brown clay cortex. Magnetometric measurements may not identify solution pipes with more sandy filling based on macroscopic analysis, which correlates with a lesser amount of clays. There was also the smallest pipe – C, on the northwestern edge of the grid. It was detected only on GPR data, and the magnetic grid did not cover it. It is similar to the giant pipe, also filled with the sandy material.

4.2.3 Grid 3

Grid 3 was the largest grid, forming a rectangle of 11.5 m × 12.5 m. The grid floor was covered with a thin layer of anthropogenically deposited sand and several clayey spots (Figure 11b). Due to this cover, the solution pipes were initially invisible. We removed the surface immediately after the measurements for two reasons. One is to provide more realistic measurement circumstances. The second is to ensure that the interpretation of the positions of the pipes based on the signal correlated with the accurate positions of the pipes. Only after the measurements were recorded and analysed, we returned to the site and removed the top 20 cm of the cover with an excavator. The pipes were then visually identified, with their positions measured. As it turned out, there were ten pipes under the sand cover. GPR measurements could generally identify most pipes' positions with reasonable accuracy. The gradiometric measurements were less conclusive, with some of the pipes undetected and several false positives. However, the control measurements of Grid 1 and Grid 2 have already demonstrated that the detection of pipes by magnetic measurements depends on the presence of ferruginous clayey and silty fill, mainly present in the cortex sediment. The core of the pipes, which dominates in their upper part, is sandier and less ferruginous and thus harder to detect.

Another feature of the magnetic gradiometry results is a rather strong signal associated with pipes of a relatively small diameter. As mentioned in the previous paragraph, such pipes are dominated by the clay cortex that lines the walls, with a higher percentage of clay minerals and iron oxides. Since the pipes have different depths throughout the research area, smaller pipes with (only) this kind of material can also be the lower remnants of once larger pipes, with their upper parts eroded or stripped away due to quarrying.

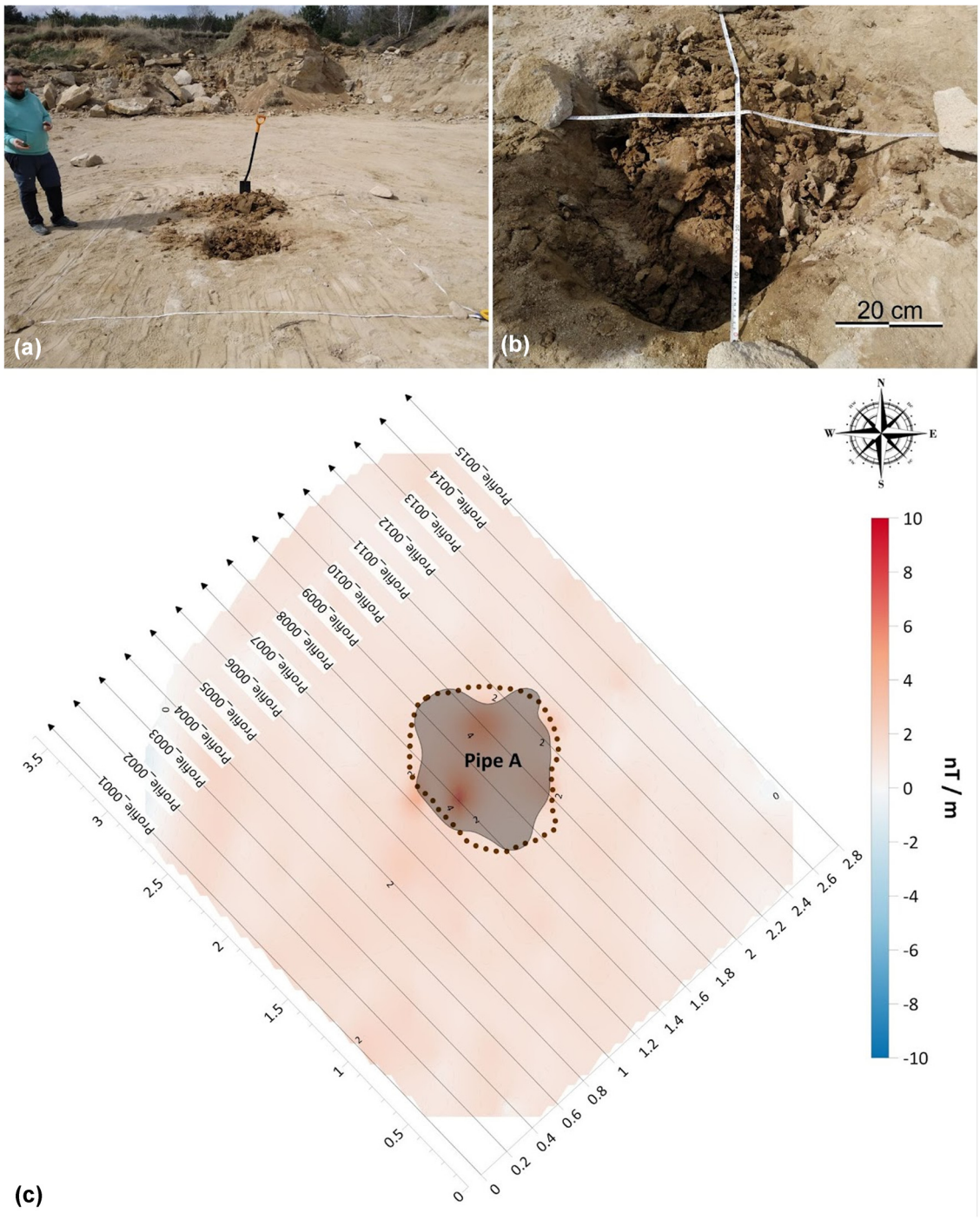

Figure 9: Grid 1, limited by tapes, with excavated single solution pipe (a), spatial dimensions of the solution pipe (b), and the spatial distribution of the vertical magnetic gradient (colour relief map) plotted with the GPR anomalies (marked by grey shaded area) and identified pipe positions (brown outlines) of Grid 1 (c). The values on the *x*, *y* axes are in metres.

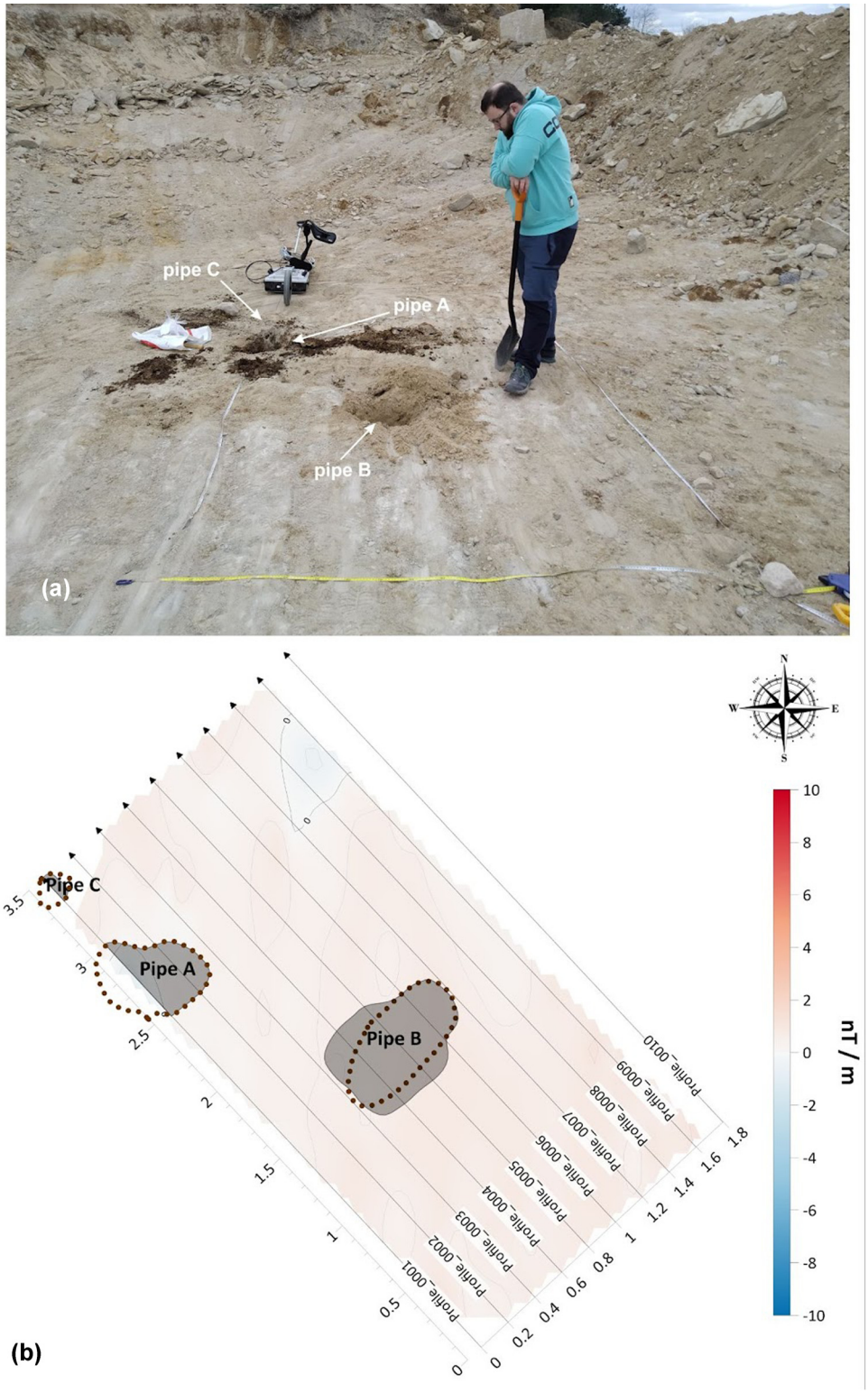

Figure 10: Grid 2, limited by tapes, with excavated solution pipes (a), and magnetic gradient (colour relief map) plotted with the GPR anomalies (marked by grey shaded areas) (b). The values on the *x*, *y* axes are in metres.

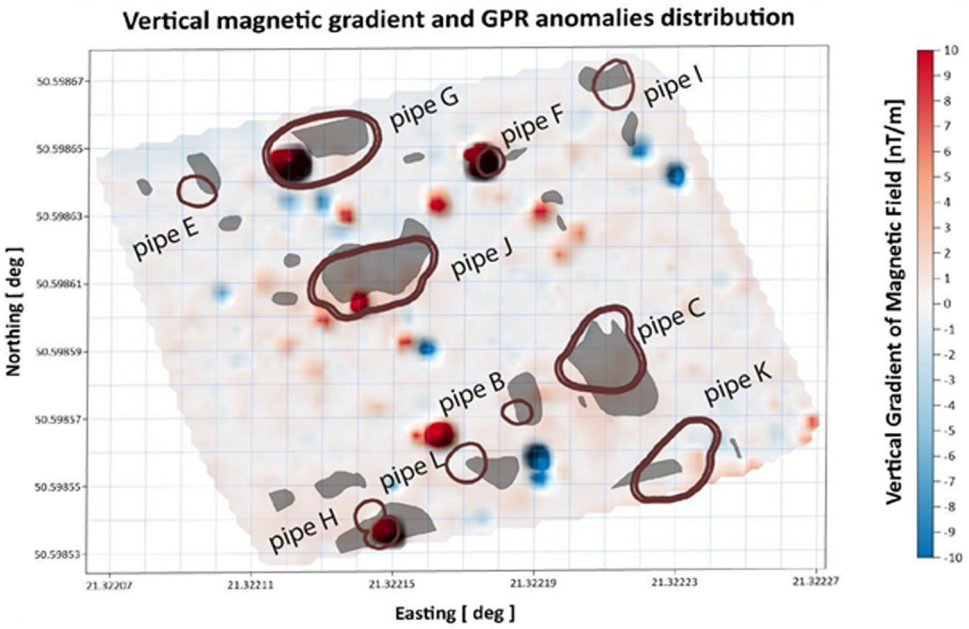

Figure 11: Grid 3 – the spatial distribution of the vertical magnetic gradient plotted (colour relief map) with overlaid GPR anomalies (marked by grey shaded areas) and identified pipe positions (brown outlines).

Slight displacements of GPR, magnetics and *in situ* detected pipes plotted on the grid (Figure 11) are due to several reasons. First, the detection of pipes in the field was done after the excavator removed the upper layer to reveal a fresh exposure. The lateral shapes of the pipes may vary with depth, which can influence the results. Second, the pipes are only sometimes completely vertical. A slight inclination results in the displacement of the magnetics detection towards the iron-rich material concentration (accumulated preferably at the bottom of the pipes) compared to the detection of pipe filling in the upper part with the GPR method. The plotted results of GPR and magnetic gradiometry measurements of Grid 3 (Figure 11) also show scattered small areas of signal attenuation and higher or lower magnetic intensity. These small areas might appear due to the presence of clayey spots on the quarry's floor and scattered excavated sediments from the surrounding pipes that do not represent the pipes themselves.

Full and proper geophysical characterisation of this area might help to understand the dissolution process and physical conditions of the formation of solution pipes. The research of solution pipes is important because they can provide information about the paleoenvironment and past climate change [42–44]. Dissolution in carbonate deposits can also cause subsidence or collapse [45]. Non-invasive geophysical surveys can be very helpful in these investigations. As shown in this article, geophysical surveys can help locate and identify even small-sized pipes.

5 Conclusions

We have demonstrated that geophysical methods can detect solution pipes in natural settings. GPR caught most of the pipes due to the significant differences in attenuation of the electromagnetic signal between the rock matrix and the pipe filling. The magnetic gradiometry measurements were less reliable because of their sensitivity to the iron concentration in the filling, which is highly heterogeneous in both horizontal and vertical directions over the research area. It should be remembered that only shallow, near-surface structures were studied, which facilitated their detection with the methods used. High dielectric constant contrast was expected as these pipes are filled with clay and surrounded by calcarenite. Therefore, the GPR method proved to be convenient in detecting them. It should be remembered that only shallow near-surface structures are studied, which should facilitate their detection with the methods used.

Measurements such as those reported here help investigate quasi-spatial correlations between pipe positions, distribution of inter-pipe distances, or a potential relationship between alignments of rock joints and pipe locations. This kind of information cannot be obtained from the

analysis of the quarry wall, as it provides only two-dimensional data.

Moreover, the magnetic survey is less effective than GPR for detecting clay-filled solution pipes. The combination of both methods demonstrated the ability for determining the pipe filling material for pipes that were detected by GPR.

The geophysical methods used in this research allowed only the determination of two-dimensional variability and horizontal mapping of solution pipes. However, they did not provide information about their vertical dimensions, which may be the subject of future research.

Acknowledgements: We cordially thank Matej Lipar and Piotr Szymczak for the consultations and permission to access the quarry. This research was funded by SEG Foundation as part of the "SEG Field Camp 2020" project.

Conflict of interest: Sebastian Kowalczyk is an editor in Open Geosciences and was not involved in the review process of this article.

References

[1] Bakalowicz M. Karst groundwater: a challenge for new resources. Hydrogeol J. 2005;13(1):148–60.
[2] Jones WK. Physical structure of the epikarst. Acta Carsol. 2013;42(2–3):311–4. doi: 10.3986/ac.v42i2-3.672.
[3] Chalikakis K, Plagnes V, Guerin R, Valois R, Bosch FP. Contribution of geophysical methods to karst-system exploration: an overview. Hydrogeol J. 2011;19(6):1169–80.
[4] Carrière SD, Chalikakis K, Sénéchal G, Danquigny C, Emblanch C. Combining electrical resistivity tomography and ground penetrating radar to study geological structuring of karst unsaturated zone. J Appl Geophysics. 2013;94:31–41.
[5] Kaufmann O, Deceuster J. Detection and mapping of ghost-rock features in the Tournaisis area through geophysical methods–an overview. Geologica Belgica. 2014;17:17–26.
[6] Verdet C, Sirieix C, Marache A, Riss J, Portais J-C. Detection of undercover karst features by geophysics (ERT) Lascaux cave hill. Geomorphology. 2020;360:107–77.
[7] Ebong ED, George AM, Ekwok SE, Akpan AE, Asfahani J. 2D electrical resistivity inversion and ground penetrating radar investigation of near surface cave in New Netim area, south-eastern Nigeria. Acta Geod Geophys. 2021;56:765–80.
[8] Xiaojun Z, Huang J, Song L, Chen Y. Application of Ground-penetrating Radar (GPR) exploration in Karst mountain areas. Proceedings of the XIII International Conference on Ground Penetrating Radar. IEEE; 2010.
[9] Hussain Y, Uagoda R, Borges W, Prado R, Hamza O, Cárdenas-Soto M, et al. Detection of cover collapse doline and other Epikarst features by multiple geophysical techniques, case study of Tarimba cave, Brazil. Water. 2020;12(10):2835.
[10] Oryński S, Okoń M, Klityński W. Very low frequency electromagnetic induction surveys in hydrogeological investigations; Case study from Poland. Acta Geophysica. 2016;64:2322–36.
[11] Klityński W, Oryński S, Dinh CN. Application of the conductive method in the engineering geology: Ruczaj district in Kraków, Poland, as a case study. Acta Geophysica. 2019;67:1791–8.
[12] Lipar M, Szymczak P, White SQ, Webb JA. Solution pipes and focused vertical water flow: Geomorphology and modelling. Earth-Sci Rev. 2021;218(7):103635.
[13] Lipar M, Szymczak P, Ciglič R, Prakash Sharma R, Zorn M, Stepišnik U, et al. Challenges in characterisation and mapping of solution pipes. EGU General Assembly 2022, Vienna, Austria, 23–27 May 2022. EGU22-1619.
[14] Pipan M, Baradello L, Forte E, Prizzon A. GPR study of bedding planes, fractures, and cavities in limestone. Proc. SPIE 4084, Eighth International Conference on Ground Penetrating Radar; 2000.
[15] Saintenoy A, Senechal G, Rousset D, Brigaud B, Pessel M, Zeyen H. Detecting faults and stratigraphy in limestone with Ground-Penetrating Radar: A case study in Rustrel. 9th International Workshop on Advanced Ground Penetrating Radar (IWAGPR); 2017.
[16] Boubaki N, Saintenoy A, Kowalczyk S, Mieszkowski R, Welc F, Budziszewski J, et al. Ground-penetrating radar prospection over a gallery network resulting from neolithic flint mine (Borownia, Poland). 14th International Conference on Ground Penetrating Radar (GPR). Shanghai; 2012. p. 610–5.
[17] Collins ME, Puckett WE, Schellentrager GW, Yust NA. Using GPR for micro-analyses of soils and karst features on the Chiefland Limestone Plain in Florida. Geoderma. 1990;47(1–2):159–70.
[18] Collins ME, Cum M, Hanninen P. Using ground-penetrating radar to investigate a subsurface karst landscape in north-central Florida. Geoderma. 1994;61(1–2):1–15.
[19] Kruse SE, Schneider JC, Campagna DJ, Inman JA, Hickey TD. Ground penetrating radar imaging of cap rock, caliche and carbonate strata. J Appl Geophysics. 2000;43:239–49.
[20] Anchuela ÓP, Casas-Sainz AM, Soriano MA, Pocoví-Juan A. Mapping subsurface karst features with GPR: results and limitations. Env Geol. 2009;58:391–9.
[21] Gómez-Ortiz D, Martín-Crespo T. Assessing the risk of subsidence of a sinkhole collapse using ground penetrating radar and electrical resistivity tomography. Eng Geol. 2012;149–150:1–12.
[22] Mount GJ, Comas X, Wright WJ, McClellan MD. Delineation of macroporous zones in the unsaturated portion of the Miami Limestone using ground penetrating radar, Miami Dade County, Florida. J Hydrol. 2015;527:872–83.
[23] Kaufmann G, Romanov D. The Jettencave, Southern Harz Mountains, Germany: Geophysical observations and a structural model of a shallow cave in gypsum/anhydrite-bearing rocks. Geomorphology. 2017;298:20–30.
[24] Bernatek-Jakiel A, Kondracka M. Detection of soil pipes using ground penetrating radar. Remote Sens. 2019;11:1864.
[25] Breiner S. Applications manual for portable magnetometers. GeoMetrics. PaloAlto USA; 1973. p. 17–32, 39–57.
[26] Hood PJ, Holroyd MT, Mcgrath PH. Magnetic methods applied to base metal exploration, in Geophysics and Geochemistry in the Search for Metallic Ores. In: Hood PJ, editor. Geological

Survey of Canada, Economic Geology Report. Vol. 31; 1979. p. 77–104.
[27] Reynolds JM. An introduction to applied and environmental geophysics. 2nd edn. Oxford, UK: Wiley-Blackwell; 2011. ISBN: 978-0-471-48535-3.
[28] Bojdys G, Cianciara B, Grabowska T, Koblański A, Małoszewski S, Marchewka A, et al. Kompleksowe badania geofizyczne żyły kwarcowej w rejonie Rozdroża Izerskiego. Zesz Nauk AGH, Geologia. 1972;312(16):27–52 [in Polish].
[29] Łój M, Gołębiowski T, Porzucek S. Geophysical surveys and modelling for recognizing of gypsum karst. Geoinformatica Polonica. 2014;13:83–97.
[30] Blazejczyk K. Climate and bioclimate of Poland. In: Degórski M, editor. Natural and human environment of Poland. A geographical overview. 2006. Warsaw: Polish Geographical Society. p. 31–48.
[31] Alexandrowicz SW, Garlicki A, Rutkowski J. Podstawowe jednostki litostratygraficzne miocenu zapadliska przedkarpackiego. Kwartalnik Geologiczny. 1982;26:470–1.
[32] Leszczyński S, Nemec W, Hampson G. Dynamic stratigraphy of composite peripheral unconformity in a foredeep basin. Sedimentology. 2015;62(3):645–80.
[33] Walsh P, Morawiecka-Zacharz I. A dissolution pipe palaeokarst of mid-Pleistocene age preserved in Miocene limestones near Staszow, Poland. Palaeogeogr Palaeoclimatol Palaeoecol. 2001;174(4):327–50.
[34] Roniewicz P, Wysocka A. Remarks on Miocene sedimentation in the area between Szydlow and Smerdyna, southeastern margin of the Holy Cross Mts (Central Poland). Przegląd Geologiczny. 2001;49(7):639–42 (in Polish with English summary).
[35] Bugajska-Pająk A. Charakterystyka surowcowa wapieni lekkich miocenu południowego obrzeżenia Gór Świętokrzyskich [Raw material characteristic of light limestones from the Miocene of southern margin of the Holy Cross Mountains]. Przegląd Geologiczny. 1974;22(9):416–21 (in Polish with English summary).
[36] Romanek A, Słowiok G. Objaśnienia do Szczegółowej mapy geologicznej Polski, Arkusz, Klimontów 1:50,000 (887) [Explanation to the detailed geological map of Poland, Kimontów, Sheet No. 887]. Wyd Geol, Warsz; 1977.
[37] Mycielska E. Formy krasowe na północ od Osieka Sandomierskiego Karstic Forms North of Osiek Sandomierski. Przegląd Geograficzny. 1960;23(4):575–85 (in Polish with English summary).
[38] Mycielska-Dowgiałło E. Rozwój geomorfologiczny południowo – wschodniej części Wyżyny Sandomierskiej w górnym miocenie i pliocenie The geomorphological evolution of the south-east part of the Sandomierz Upland in the upper Miocene and Pliocene. Przegląd Geograficzny. 1965;37(4):637–49 (in Polish with English summary).
[39] Morawiecka I, Walsh P. A study of solution pipes preserved in the Miocene limestones (Staszów, Poland). Acta Carsol. 1997;26(2):337–50.
[40] Sandmeier KJ. ReflexW (version 7.5) program for the processing of seismic, acoustic or electromagnetic reflection, refraction and transmission data. Karlsruhe, Germany: Sandmeier; 2015.
[41] Blundell SJ, Poirier A. Magnetic properties of clay minerals. Rev Mineral Geochem. 1991;23(1):181–228.
[42] Lipar M, Webb JA, White SQ, Grimes KG. The genesis of solution pipes: Evidence from the Middle–Late Pleistocene Bridgewater Formation calcarenite, southeastern Australia. Geomorphology. 2015;246:90–103.
[43] Pound MJ, McCoy J. Palaeoclimate reconstruction and age assessment of the Miocene flora from the Trwyn y Parc solution pipe complex of Anglesey, Wales, UK. Palynology. 2021;45(4):697–703.
[44] Valera-Fernández D, Solleiro-Rebolledo E, López-Martínez R, Sedov S, Griset S, Cabadas-Báez H. Quaternary paleoenvironments based on pedogenic, sedimentary and karstic processes in the coastal geosystems of Cozumel Island, Mexico. Geoderma Regional. 2022;31:e00587.
[45] Edmonds, CN. Chapter 15 Dissolution – carbonates. Geol Society London, Eng Geol Spec Publ. 2020;29(1):389–401.